Sliding Mode Control in a Two Axis Gimbal System

Brian J. Smith William J. Schrenk William B. Gass
United States Army Aviation and Missile Command
ATTN: AMSAM-RD-SS-AA
Redstone Arsenal, Alabama 35898
256-876-1330
brians@redstone.army.mil

Yuri B. Shtessel
Department of Electrical and Computer Engineering
University of Alabama in Huntsville
Huntsville, Alabama 35899
256-890-6164
shtessel@ebs330.eb.uah.edu

Abstract–This paper considers the performance of a two-axis gimbal system, which is typical of surface-to-air, air-to-air, and air-to-surface tactical missiles, when Sliding Mode Control is utilized. A representative gimbal system consisting of a flat planar antenna, pitch/yaw gimbals, connecting push rods, and separate armature controlled DC drive motors for the pitch and yaw gimbals is utilized to develop the theory and to serve as a testbed for digital simulation. The equations describing the gimbal system under consideration are highly nonlinear and include terms which are not accurately known or can not be accurately measured during the missile's flight. It is shown that the use of variable structure control or sliding mode control can be used to provide robust seeker performance in the face of non-linearity's and uncertainties.

TABLE OF CONTENTS

1. INTRODUCTION

The majority of contemporary tactical missile systems utilize a gimbaled seeker. The control technique used for the gimbal system on a tactical missile must provide rapid and accurate tracking of boresight error signals generated by the missile's signal processing unit. Demands on the control system are most severe during the endgame portion of the missile's flight. Poor performance during endgame will result in large miss distances and a corresponding low probability of mission success.

The equations describing the gimbal system under consideration are highly nonlinear and include terms which are not accurately known or can not be accurately measured during the missile's flight. It is shown that the use of variable structure control or sliding mode control can be used to provide robust seeker performance in the face of non-linearities and uncertainties [1,2].

2. BACKGROUND

The "Antenna Servo" unit positions the antenna in response to control signals, which may be provided either by 1) search scan circuitry in the indicator, or by 2) the angle tracking system [3]. A separate servo channel is provided for each gimbal. The voltage obtained from a transducer on the gimbal is subtracted from the control signal, thereby producing an error signal proportional to the error in the antenna's position. Classical control theory has been used for antenna control with system response improved by the following basic categories using frequency domain techniques [4]: series (cascade) compensation, feedback (parallel) compensation, and load compensation. Contemporary control theory has been applied to stabilization of a three-axis inertial platform in [5].

3. PROBLEM FORMULATION

Figure 1(a) illustrates the problem under consideration. The antenna receives some signal from the target and after processing by the missile's signal processing unit, a boresight error signal is produced. It is the job of the gimbal control unit to drive this error to zero. Depending on the guidance law used by the missile (pursuit, proportional navigation, etc.) the orientation of the missile in inertial space will also be changed. However, in this paper the closed loop performance of the missile is not evaluated.

The overall objective of the gimbal control system is to follow a desired trajectory developed in real-time as rapidly as possible with minimum steady state error. A side view of the gimbal system is shown in Figure 1(b). Figure 1(b) shows rotation about the Y_G axis, which is referred to as the pitch channel. The antenna plate is rotated about the Y_G axis by an armature controlled DC motor through a push rod assembly. The length l in Figure 1(b) is held constant by allowing the point (P) to slide along the antenna plate as required. The yaw channel is identical to the pitch channel, but with rotation about the Z_G axis. In other words, it is orthogonal to the pitch channel. The antenna does not rotate about the X_G axis, i.e. there is no roll. One set of axes is fixed to the top of the gimbal support post and

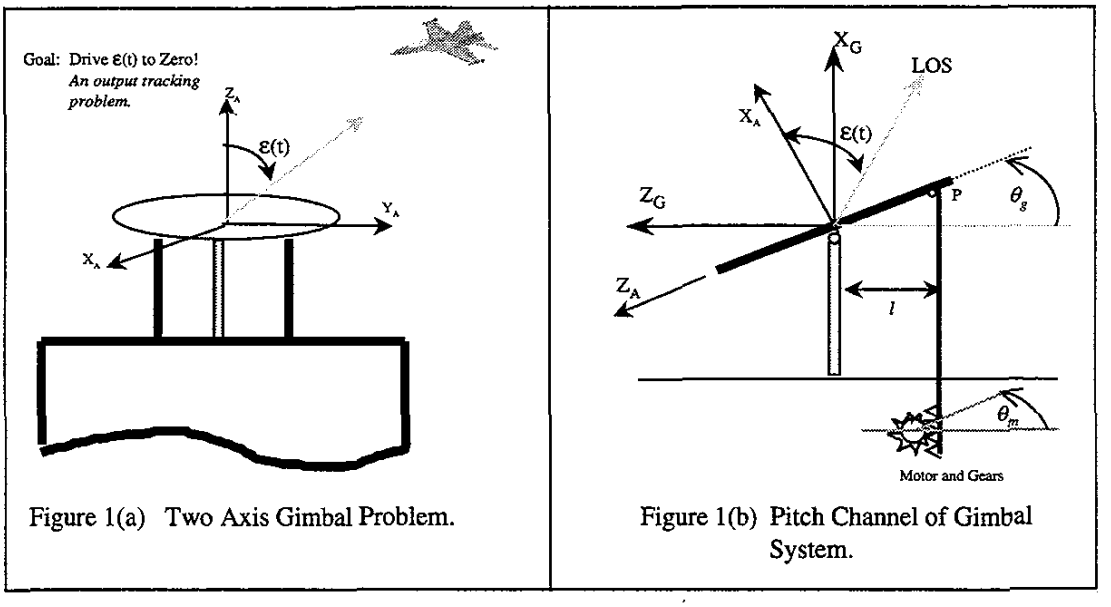

Figure 1(a) Two Axis Gimbal Problem.

Figure 1(b) Pitch Channel of Gimbal System.

Figure 1 Missile Seeker Gimbal System

another to the antenna. When the antenna is at its home position the gimbal support (X_G, Y_G, Z_G) and the antenna (X_A, Y_A, Z_A) axes are in alignment.

The rotational motion of the antenna has been modeled using Euler's equations of motion [6]. To simplify the analysis of the gimbal system, the equations of motion have been written relative to an inertial frame. However, to fully model the performance of a gimbal for a missile in flight, the equations of motion must be modified to take into account the missile's dynamics. A judicious reference frame choice allows the rotational motion of a rigid body to be modeled as

$$\begin{aligned} \tau_x &= I_{xx}\dot{\omega}_x + (I_{zz} - I_{yy})\omega_y\omega_z \\ \tau_y &= I_{yy}\dot{\omega}_y + (I_{xx} - I_{zz})\omega_z\omega_x \\ \tau_z &= I_{zz}\dot{\omega}_z + (I_{yy} - I_{xx})\omega_x\omega_y \end{aligned} \tag{1}$$

The antenna is modeled as a circular plate so the moments of inertia are given as

$$\begin{aligned} I_{xx} &= I_{yy} = \tfrac{1}{4} m r_A^{\,2} \\ I_{zz} &= \tfrac{1}{2} m r_A^{\,2} \end{aligned} \tag{2}$$

Noting that $\omega_z = 0$ and using eq (2) in eq (1) results in

$$\begin{aligned} \tau_x &= I_{xx}\dot{\omega}_x \\ \tau_y &= I_{yy}\dot{\omega}_y \\ \tau_z &= 0 \end{aligned} \tag{3}$$

From eq (3) it is seen that the pitch and yaw channels are not coupled. Taking into account viscous damping, friction, and the torques generated by the missile's motion eq (3) becomes

$$\begin{aligned} \tau_x &= I_{xx}\ddot{\theta}_{gx} + f_x\dot{\theta}_{gx} + F_x + \xi_x(t) \\ \tau_y &= I_{yy}\ddot{\theta}_{gy} + f_x\dot{\theta}_{gy} + F_y + \xi_y(t) \\ \tau_z &= 0 \end{aligned} \tag{4}$$

where

f_x, f_y - viscous damping coefficients
F_x, F_y - friction (static and sliding)
$\xi_x(t), \xi_y(t)$ - torques produced on the antenna due to missile motion.

The viscous damping coefficients (f_x, f_y) are readily determined. The friction coefficients (F_x, F_y) and torques ($\xi_x(t)$, $\xi_y(t)$) however, are dynamic and are not easily determined during the missile's flight. Therefore they will be treated as unknown disturbances. It is assumed that only their maximum values are known.

A block diagram for an armature controlled DC motor is given in Figure 2(a). For our investigation we will assume that the "electrical time constant" L/R is much smaller than the "mechanical time constant" J_m/B_m. This is a reasonable assumption for many electro-mechanical systems and leads to a reduced order model as shown in Figure 2(b) [7]. In Figure 2(b) τ_l is the torque caused by the gimbal system

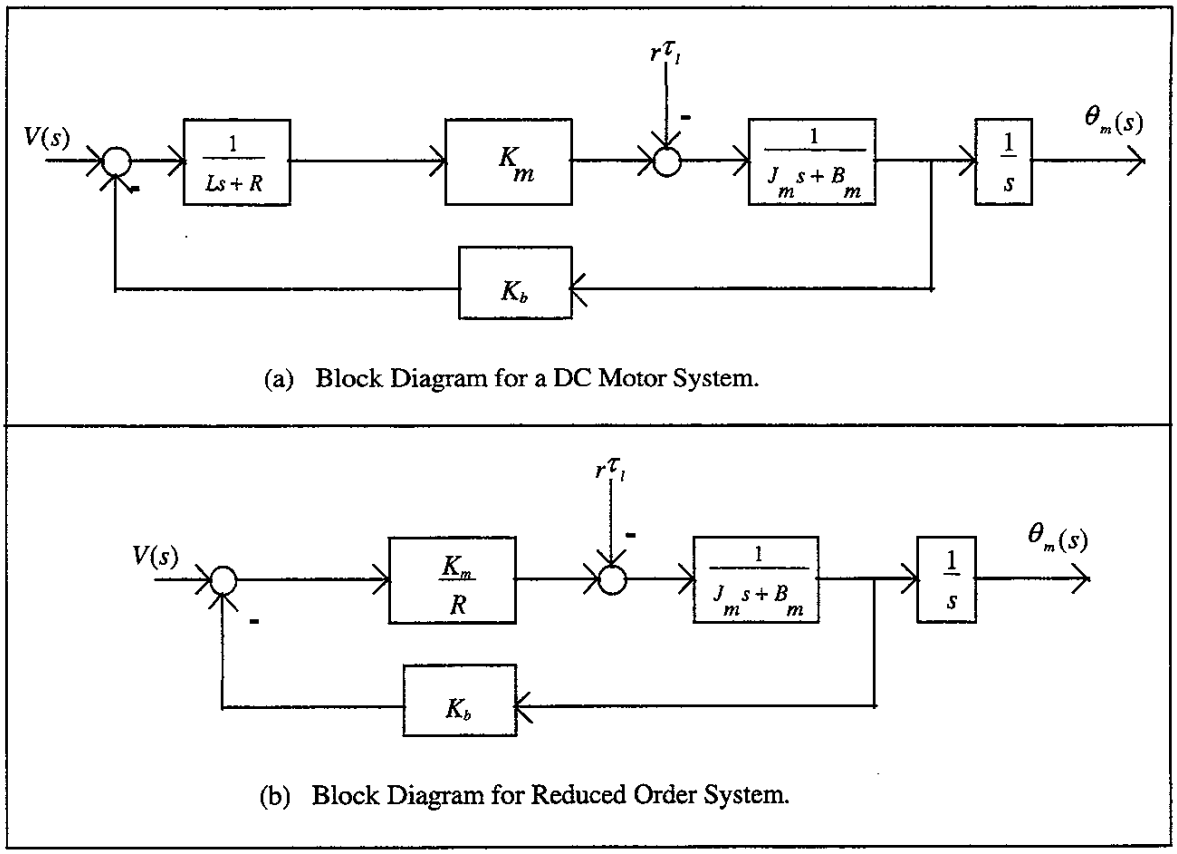

Figure 2 Model of a DC Motor Used in the Gimbal System

eq (4). In the time domain the differential equation describing the simplified motor model is

$$J_m \ddot{\theta}_m(t) + (B_m + \frac{K_b K_m}{R})\dot{\theta}_m(t) = (\frac{K_m}{R})V(t) - r\tau_l(t) \quad (5)$$

where r is the gear ratio of the gear train between the motor and pushrod. Equations for the dynamics of the antenna (4) and drive motor (5) are linked by the term $\tau_l(t)$. The relation between θ_m and θ_g is given by

$$\theta_m = \frac{l}{g_r}\tan(\theta_g) \quad (6)$$

where

l - is the length given in Figure 1(b).
g_r - is the radius of the motor gear meshing with the push rod.

Since the pitch and yaw channels are uncoupled and identical, only the pitch channel will be considered in the remainder of this paper. Equations for the yaw channel can be derived in a similar manner as those of the pitch channel. Subscript symbols for x and y have been dropped in the following derivations where possible.

Substituting eq (4) in eq (5) gives

$$J_m\ddot{\theta}_m(t) + (B_m + \frac{K_b K_m}{R})\dot{\theta}_m(t) = (\frac{K_m}{R})V(t) - r[I_{xx}\ddot{\theta}_g + f\dot{\theta}_g + F + \xi(t)] \quad (7)$$

To transform eq (7) so that it is only a function of θ_g, it is necessary to find the first and second derivatives of eq (6) in terms of θ_g and use them in eq (7). The first and second derivatives of eq (6) are

$$\frac{d}{dt}(\frac{l}{g_r}\tan\theta_g) = \frac{l}{g_r}\dot{\theta}_g\sec^2\theta_g$$

$$\frac{d}{d^2t}(\frac{l}{g_r}\tan\theta_g) = \frac{l}{g_r}\sec^2\theta_g[\ddot{\theta}_g + 2\dot{\theta}_g{}^2\tan\theta_g] \quad (8)$$

Using eq (8) for the first and second derivatives of θ_m, in terms of θ_g, in eq (7) results in the following relationship for the combined antenna and motor dynamics in terms of θ_g

$$
\begin{aligned}
&[J_m \frac{l}{g_r}\sec^2\theta_g + rI_{xx}]\ddot{\theta}_g \\
&+[2J_m \frac{l}{g_r}\dot{\theta}_g \sec^2\theta_g \tan\theta_g + (B_m + \frac{K_b K_m}{R})\frac{l}{g_r}\sec^2\theta_g + rf]\dot{\theta}_g \\
&+[rF + r\xi(t)] \;=\; \frac{K_m}{R}V(t)
\end{aligned}
\tag{9}
$$

The differential equation (9) can be transformed to a state variable description using the following relationships

$$
\begin{aligned}
x_1 &= \theta_g \\
x_2 &= \dot{\theta}_g
\end{aligned}
\tag{10}
$$

The use of eq (10) transforms eq (9) into the following state variable form

$$
\begin{aligned}
\dot{x}_1 &= x_2 \\
\dot{x}_2 &= \frac{1}{J_m \frac{l}{g_r}\sec^2(x_1) + rI_{xx}}\Big\{-[2J_m \frac{l}{g_r}x_2 \sec^2(x_1)\tan(x_1) \\
&\qquad + (B_m + \frac{K_b K_m}{R})\frac{l}{g_r}\sec^2(x_1) + rf]x_2 \\
&\qquad -[rF + r\xi(t)] + \frac{K_m}{R}V(t)\Big\} \\
y &= x_1
\end{aligned}
\tag{11}
$$

where y is the output of interest. For the following computations let

$$
\begin{aligned}
\varphi(x_1,x_2) &= \frac{1}{J_m \frac{l}{g_r}\sec^2(x_1) + rI_{xx}}\Big\{-[2J_m \frac{l}{g_r}x_2 \sec^2(x_1)\tan(x_1) \\
&\qquad + (B_m + \frac{K_b K_m}{R})\frac{l}{g_r}\sec^2(x_1) \\
&\qquad + rf]x_2 - [rF + r\xi(t)]\Big\}
\end{aligned}
$$

$$
\begin{aligned}
b(x_1,x_2) &= \frac{1}{J_m \frac{l}{g_r}\sec^2(x_1) + rI_{xx}}\left\{\frac{K_m}{R}\right\} \\
U &= V(t)
\end{aligned}
\tag{12}
$$

which results in the following formulation for eq (11)

$$
\begin{aligned}
\dot{x}_1 &= x_2 \\
\dot{x}_2 &= \varphi_o(x_1,x_2) + \Delta\varphi(x_1,x_2) \\
&\qquad + \{b_o(x_1,x_2) + \Delta b(x_1,x_2)\}U \\
y &= x_1
\end{aligned}
\tag{13}
$$

The quantity $\varphi_o(x_1,x_2)$ is the nominal value of $\varphi(x_1,x_2)$ given in eq (12). This is the value assuming all of the motor parameters, moments of inertia, and other values are known. The parameters F and $\xi(t)$ of eq (12) are not included in $\varphi_o(x_1,x_2)$. The variable $\Delta\varphi(x_1,x_2)$ represents deviations in the nominal values of $\varphi(x_1,x_2)$ and the disturbances F and $\xi(t)$. The definitions of $b_o(x_1,x_2)$ and $\Delta b(x_1,x_2)$ are similar where $b_o(x_1,x_2)$ is the nominal value of $b(x_1,x_2)$ in eq (12) and $\Delta b(x_1,x_2)$ represents the unknown variations in the nominal values.

4. Sliding Manifold and Control Design

A sliding mode controller design consists of two steps. In the first step a sliding surface is chosen such that the closed loop system motion on this surface exhibits a desired behavior regardless of plant uncertainties and disturbances. In the second step a control function is chosen to provide reaching of the sliding surface in finite time and to guarantee system motion in this surface thereafter.

Sliding Manifold Design

The system (13) is in regular form and the terms $\varphi_o(x_1,x_2)$ and $\Delta\varphi(x_1,x_2)$ are treated as matched disturbances [8]. If the desired output is denoted as y^* then the system can be written in errors as

$$
\begin{aligned}
e &= y^* - y \\
\tilde{x}_1 &= x_1^* - x_1 \\
\tilde{x}_2 &= x_2^* - x_2
\end{aligned}
\tag{14}
$$

Assuming the sliding manifold is of the form $\sigma = \tilde{x}_2 + c_1\tilde{x}_1$ then the system on the sliding surface can be written as

$$
\begin{cases}
\dot{\tilde{x}}_1 = -c_1\tilde{x}_1 \\
e = \tilde{x}_1
\end{cases}
\tag{15}
$$

The coefficient c_1 can be found by noting that the settling time of this first order differential equation is approximately equal to:

$$
\tau_s = \frac{4}{c_1}
\tag{16}
$$

If a desired settling time of 0.1 *sec* is desired then $c_1 = 40$. This results in the equation for the sliding manifold of $\sigma = \tilde{x}_2 - 40\tilde{x}_1$ in error terms.

Control Function Design

The equation for σ in the original basis is given as

$$\sigma = \dot{y}^* + 40y^* - x_2 - 40x_1 = 0 \tag{17}$$

The control law is designed using a Lyapunov based approach. The σ dynamics are derived as follows

$$\begin{aligned} \dot{\sigma} &= \ddot{e} + c_1\dot{e} = 0 \\ &= \ddot{y}^* - \varphi - \Delta\varphi + c_1\dot{e} - (b+\Delta b)U \end{aligned} \tag{18}$$

where the explicit dependence on x_1 and x_2 has been dropped in eq (18) for φ, $\Delta\varphi$, b, Δb. A review of $b(x_1,x_2)$ in eq (12) reveals that its value is always positive. Therefore, the candidate to the Lyapunov function

$$Q = \tfrac{1}{2}b^{-1}(x_1,x_2)\sigma^2 \tag{19}$$

is positive definite and its derivative is given by

$$\begin{aligned} \dot{Q} = b^{-1}\sigma[&\ddot{y}^* - \varphi - \Delta\varphi + c_1\dot{e} - (b+\Delta b)U \\ &-\tfrac{1}{2}b^{-1}\dot{b}\sigma] \end{aligned} \tag{20}$$

In order to provide asymptotic stability to the origin of the system in eq (18) the following format for the derivative of the candidate to the Lyapunov function is required

$$\dot{Q} < -\rho_1|\sigma|, \quad \rho_1 > 0 \tag{21}$$

It is well known that if the inequality in eq (21) holds true then the sliding surface defined by eq (17) will be reached in a finite amount of time.

The following control law can be utilized to asymptotically stabilize $\sigma = 0$ in eq (18)

$$U = \hat{U}_{eq} + \hat{\rho}\cdot sign(\sigma) \tag{22}$$

Where $\hat{U}_{eq}$ is an estimate of the equivalent control function U_{eq} that makes the derivative of the candidate to the Lyapunov function, eq (20) equal to zero. The equivalent control function U_{eq} is obtained from eq (20) and is given by

$$U_{eq} = [b+\Delta b]^{-1}\cdot[\ddot{y}^* - \varphi - \Delta\varphi + c_1\dot{e} - \tfrac{1}{2}b^{-1}\dot{b}\sigma] \tag{23}$$

We must utilize an estimate of U_{eq}, denoted as $\hat{U}_{eq}$ in the control law since U_{eq} contains the uncertain terms Δb and $\Delta\varphi$. The estimated equivalent control is given by

$$\hat{U}_{eq} = b^{-1}(\ddot{y}^* - \varphi + c_1\dot{e} - \tfrac{1}{2}b^{-1}\dot{b}\sigma) \tag{24}$$

The value of $\hat{\rho}$ in eq (22) is given by

$$\hat{\rho} \geq (L_1/b_{\min} + \rho)/(1-\alpha) \tag{25}$$

where;

$$\rho \geq 2\sqrt{Q(0)}/(t_r\sqrt{2b_{\min}})$$

$$L_1 \geq -\Delta\varphi - b^{-1}\Delta b(\ddot{y}^* - \varphi + c_1\dot{e} - \tfrac{1}{2}b^{-1}\dot{b}\sigma)$$

$$\alpha > b^{-1}\Delta b$$

$b_{\min}$ – minimum value of $b(x_1,x_2)$

t_r – desired reaching time

The description of the system (13) with sliding mode control is given as

$$\begin{cases} \dot{x}_1 = x_2 \\ \dot{x}_2 = \varphi_o + \Delta\varphi + (b_o + \Delta b)\cdot[\hat{U}_{eq} + \hat{\rho}\,sign(\varphi)] \\ y = x_1 \end{cases} \tag{26}$$

5. Gimbal System Simulation

The pitch axis of the gimbal system with sliding mode control is defined by eq (26) and has been simulated using an all-digital simulation. Table 1 lists the values used for system simulation. The gimbal is limited to ± 45 *deg.* of travel and the maximum value for x_2 is 90 *deg/sec.* Gimbal stops of ± 45 *deg* insure that there is not a singularity condition for $\varphi(x_1,x_2)$, $b(x_1,x_2)$ and the maximum value for angular velocity x_2 (ω) is useful for determining the maximum value of $\varphi(x_1,x_2)$.

It is assumed that the position (θ_g) and angular velocity ($\dot{\theta}_g$) of the antenna plate are measured perfectly and are available for use by the sliding mode controller for the simulation. A desired trajectory y^* used for evaluation of the developed sliding surface and control is given in Figure 3. The chosen trajectory is realistic of what a missile's seeker would encounter in trying to track a maneuvering target. At a long range from the target the boresight errors

would be relatively small however, as the missile approaches the target the boresight errors will rapidly grow. Figure 4 contains $y^*, \dot{y}^*, \text{and } \ddot{y}^*$ which are utilized by the control function. It should be noted that $y^*, \dot{y}^*, \text{and } \ddot{y}^*$ must be measured/calculated in real-time during the missile's flight. The predetermined values given in this paper are for illustrative purposes.

Table 1. Gimbal System Parameters

Variable	Value
m	0.551 *Kg*
r_A	0.1 *m*
$\max\{F_x\}$	0.5 *Nm*
f_x	9.45 Kgm^2/s
$\max\{\xi(t)\}$	0.01 *Nm*
J_m	1.0 Kgm^2
B_m	1.0 *Ns*
K_b	0.1 *Vs*
K_m	75.0 *Nm/A*
R	0.5 Ω
r	1.0 (ratio)
l	0.06 *m*
g_r	0.00635 *m*
$\hat{\rho}$	15.0 *rad/s*

Nominal Case (No Disturbances)

The first set of simulation runs is for the nominal case, i.e., $\Delta\varphi$ and Δb are zero. This is to establish a reference case to determine the degradation in system performance when disturbances are added. The state variables x_1 and x_2 for this case are given in Figure 5. The antenna was given an initial displacement of 20 deg and no initial angular velocity. The switching surface (σ) versus time is shown in Figure 6. For the case under consideration, once the sliding surface ($\sigma = 0$) is reached the system stays in the sliding mode, a desirable result. The motor voltage, designated the control U in the previous section, is given in Figure 7. Once the system reaches the sliding surface at approximately 1 sec, the voltage begins high speed switching. The culmination of the simulation is shown in Figure 8, which compares the actual antenna trajectory to the desired antenna trajectory. Figure 8 shows that once the initial displacement of the antenna with respect to the desired trajectory is compensated, the actual and desired trajectories are identical when there are no disturbances present.

System with Disturbances

One of the primary features of sliding mode controllers is their ability to operate in the presence of unknown disturbances. Figure 9 shows the $\Delta\varphi$ disturbance that was introduced to the nominal case. In addition to the disturbance shown in Figure 9 a Δb disturbance was added by reducing the motor parameter K_m by 10% five seconds into the simulation. Figure 10 shows that the disturbances did not effect the systems ability to reach the sliding surface or its ability to stay on the surface. Figure 11 shows the control U (motor voltage) for the system with disturbances. A comparison of Figures 7 and 11 reveals that the disturbances do not greatly change the character of the control signal. It is clear from Figure 12 that the disturbances do not effect the gimbal systems ability to track the target. The system is able to operate satisfactorily for reductions in K_m up to 20%. Beyond a 20% reduction the system is unable to track the reference profile.

Smooth Control

There are situations where high speed switching of the control signal is undesirable. The chattering can be removed by introducing a boundary layer about the sliding surface [9]. In this case, the system will not stay on the sliding surface but in some neighborhood about the sliding surface. The price paid for a smooth control signal is some loss in control system robustness. To eliminate chattering the $sign(\sigma)$ function in eq (26) is replaced with the $sat(\sigma)$ function. The *sat* function is shown in Figure 13 for reference. The size of the boundary layer about the sliding surface is determined by the choice of ε in Figure 13. It should be noted that

$$\lim_{\varepsilon \to 0} sat_{\varepsilon}(x) \quad \Rightarrow \quad sign(x) \tag{27}$$

For the gimbal system under consideration an ε of 50*msec* was empirically found to produce a smooth control signal and to allow the system to perform properly. Utilizing the *sat* function required an increase of $\hat{\rho}$ from 15.0 *rad/s* to 30.0 *rad/s*. Sigma versus time is shown in Figure 14 and V_m versus time is shown in Figure 15 for the smoothed case with disturbances. The antenna trajectory is shown in Figure 16 and it is clear that the control system allows the reference trajectory to be accurately tracked.

It should be noted that integration step size and integration technique are important items to consider when simulating the high speed switching in a sliding mode controller. To ensure simulation stability in these examples an integration step of 1*msec* and a first order Euler integration technique was utilized.

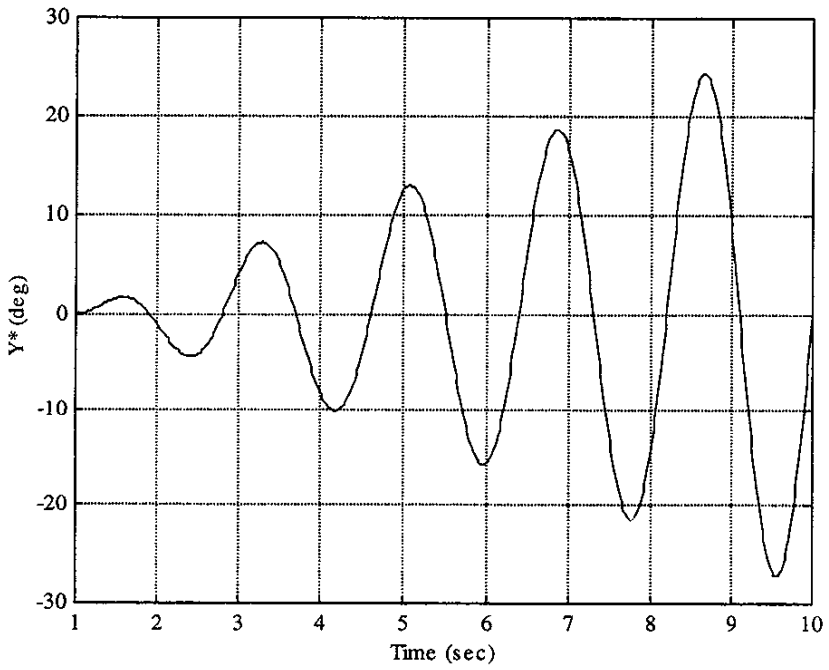

Figure 3 Desired Antenna Trajectory (y^*)

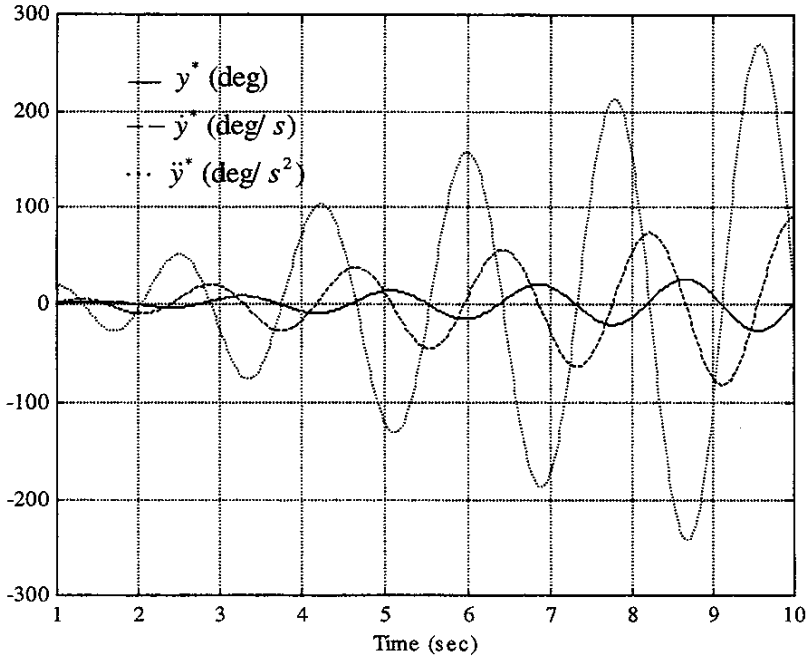

Figure 4 Desired Antenna Trajectory and its First Two Derivatives

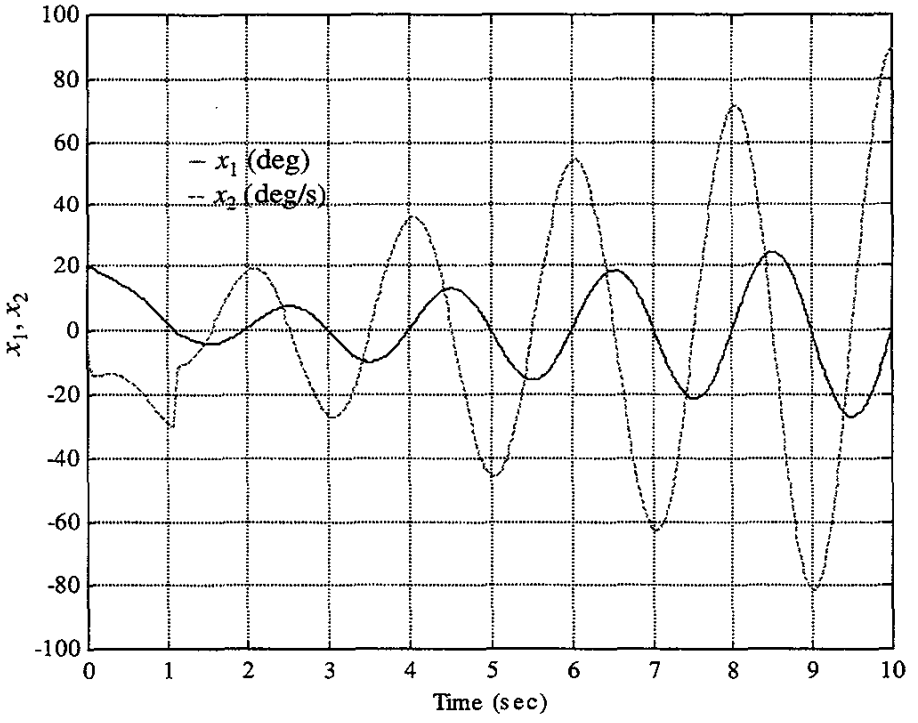

Figure 5 State Variables x_1, x_2 Versus Time $\{x_1(0) = 20, x_2(0) = 0\}$.

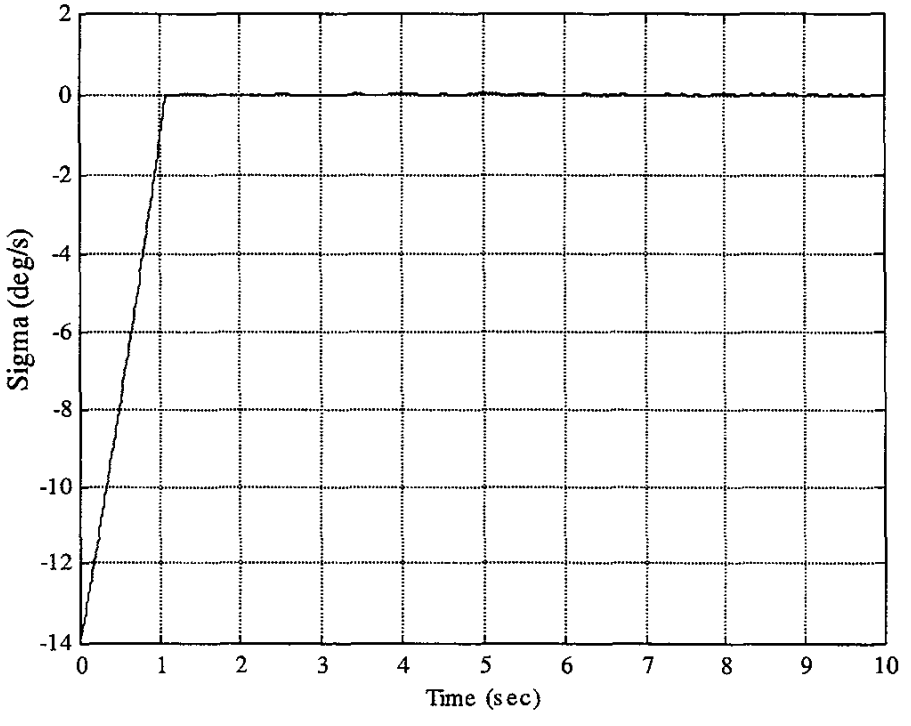

Figure 6 Sigma Versus Time.

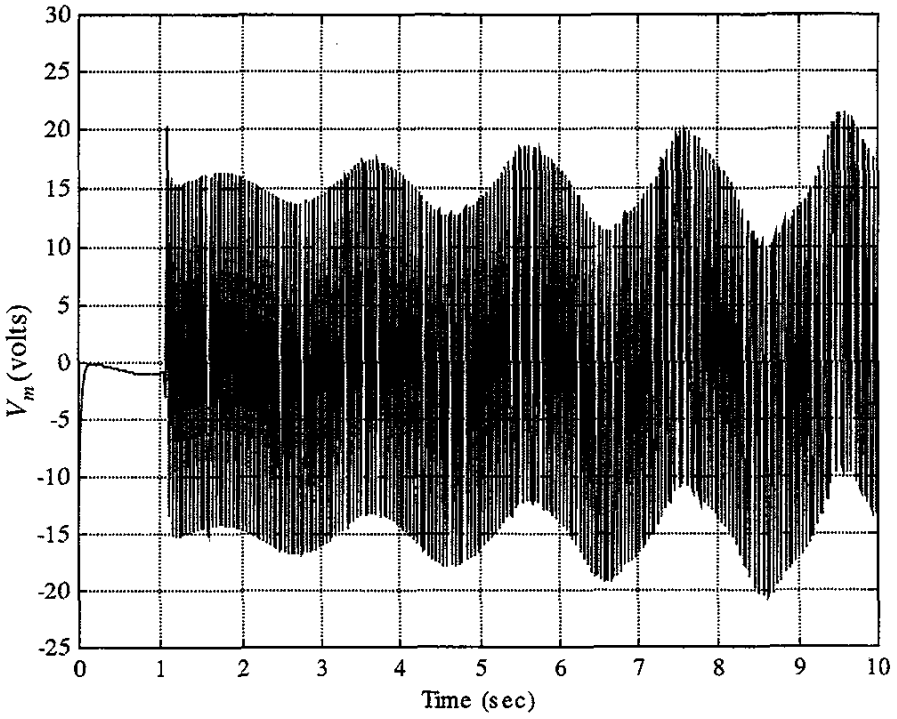

Figure 7 Motor Voltage Versus Time.

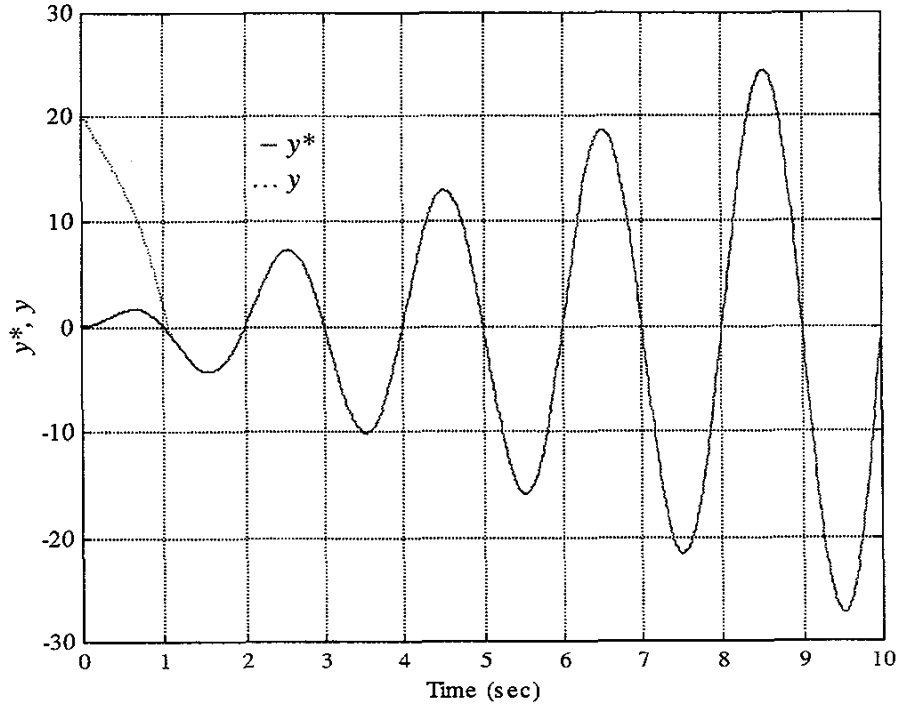

Figure 8 Desired and Actual Antenna Trajectories, Nominal Case.

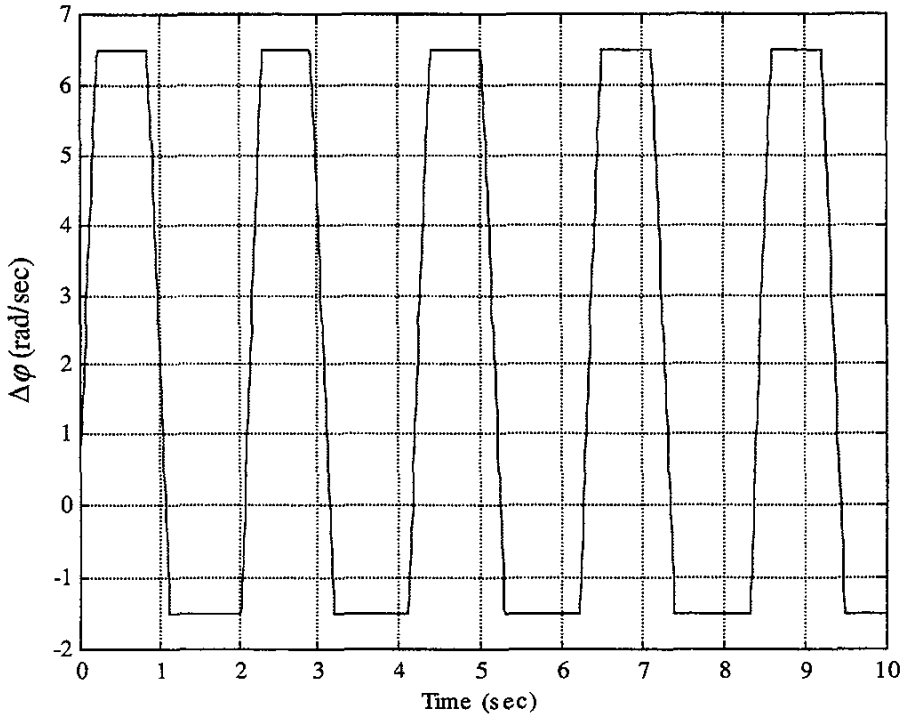

Figure 9 Disturbance Signal $\Delta\varphi(x_1,x_2)$.

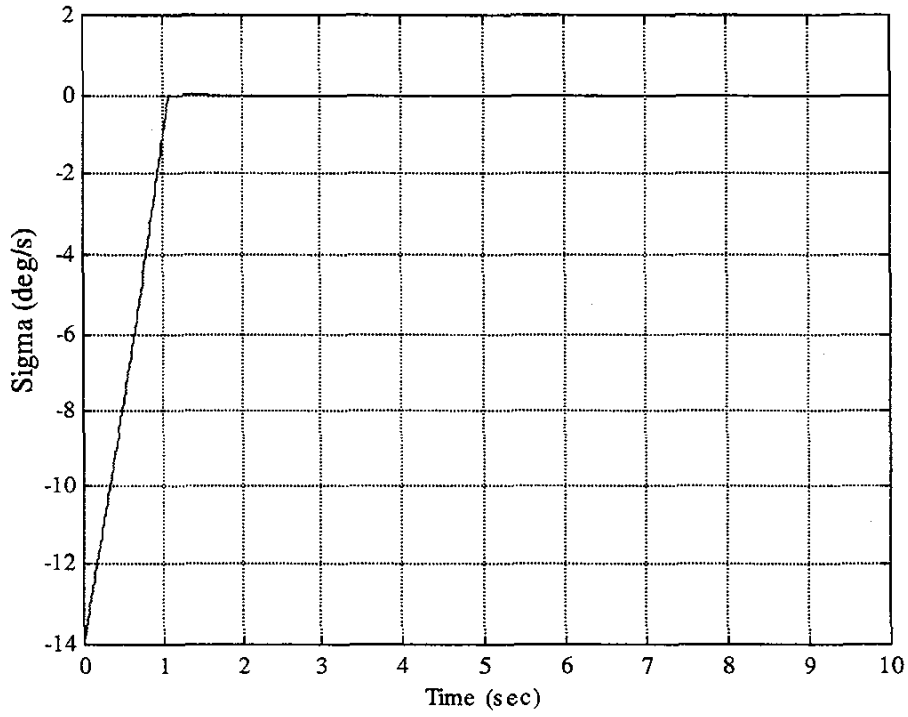

Figure 10 Sigma for the Disturbance Case.

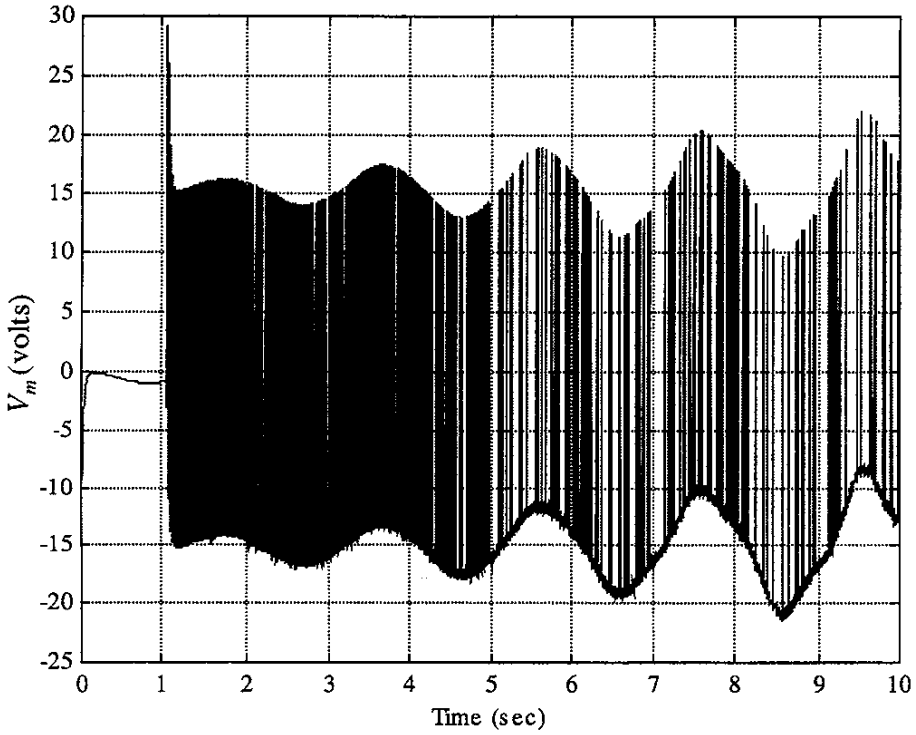

Figure 11 Motor Voltage for the Disturbance Case.

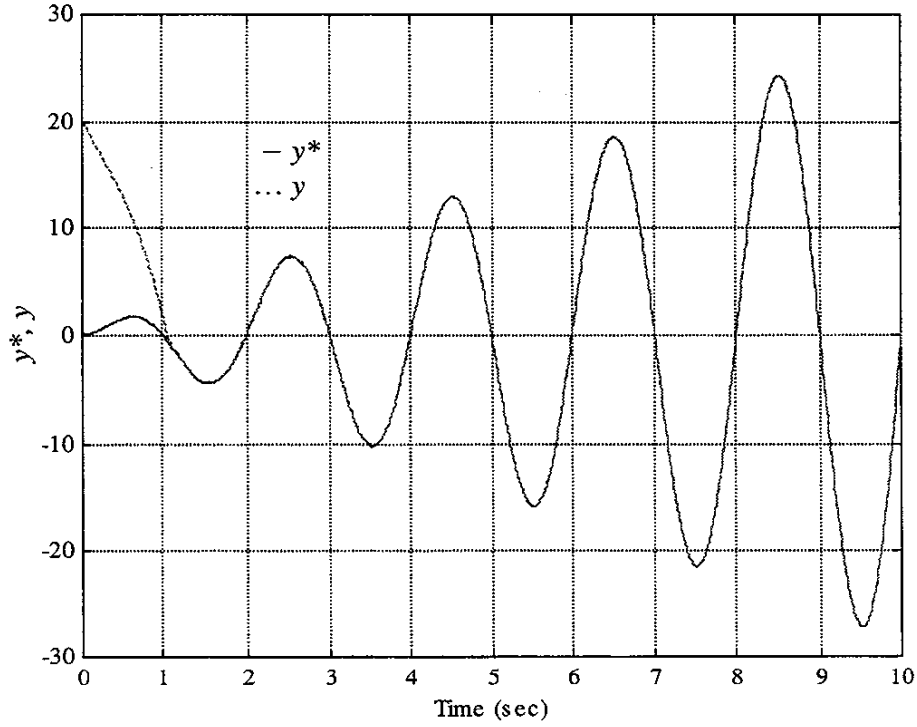

Figure 12 Antenna Trajectory for the Disturbance Case.

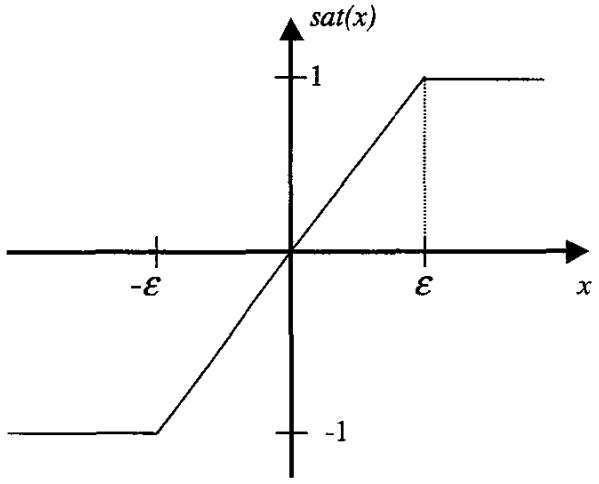

Figure 13 The *sat(x)* Function Used to Eliminate Chattering.

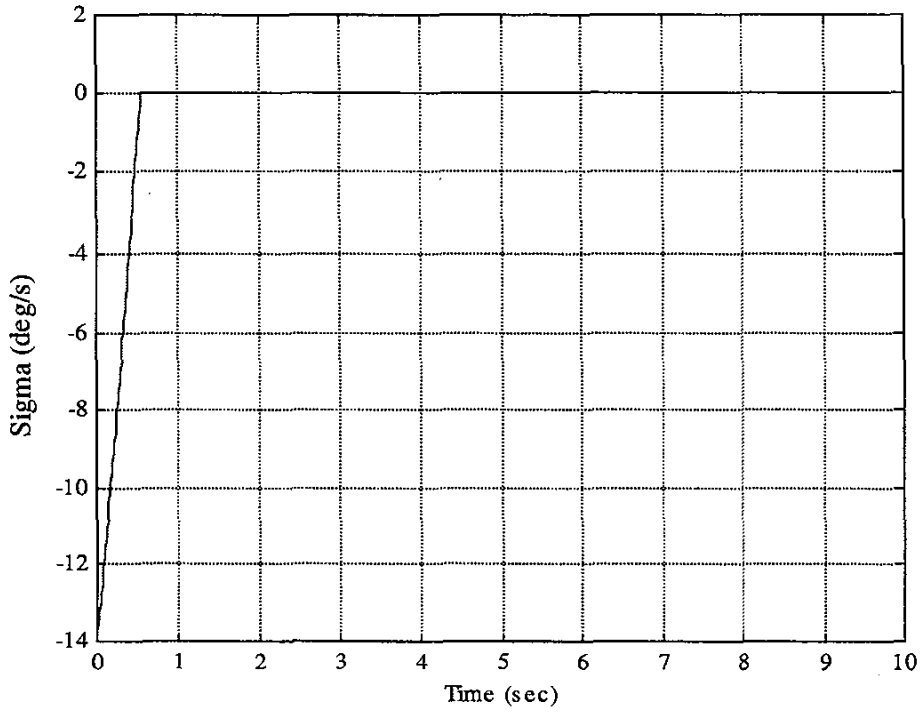

Figure 14 Sigma for *sat(σ)* Case and Disturbances.

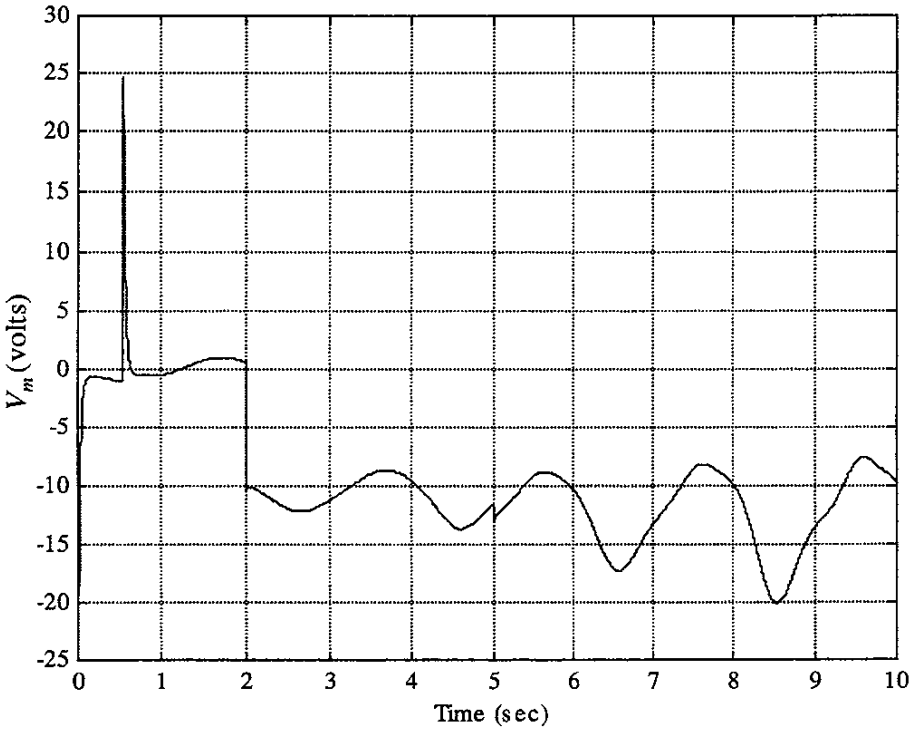

Figure 15 Motor Voltage for *sat(σ)* and Disturbance Case.

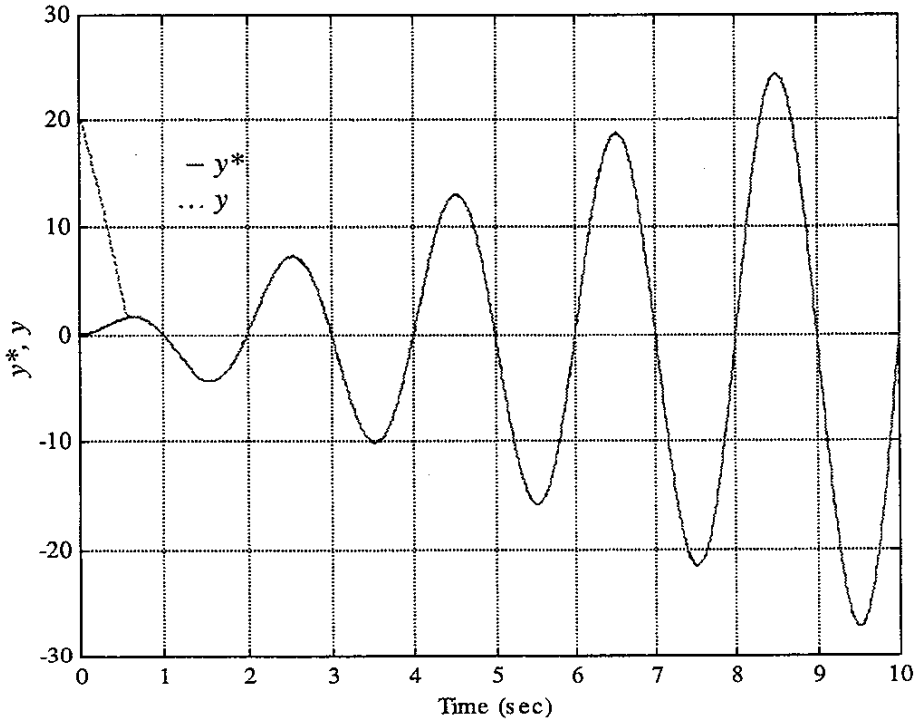

Figure 16 Antenna Trajectory for *sat(σ)* and Disturbance Case.

6. CONCLUSION

A control scheme for a two axis gimbal system based on the sliding mode control technique has been designed and validated through simulation. The derived sliding mode controller provides excellent tracking in the face of unknown or ill-defined disturbances and system parameters. In addition, realization of the developed control system is relatively simple, a fundamental attribute of the sliding mode control technique. Addition of noise on the measured values θ_g, $\dot{\theta}_g$ used for control will degrade antenna tracking performance. The extent of this degradation is dependent on the severity of the noise. Areas for future study include: refined models for the antenna moments of inertia including effects of the push-rods, incorporation of parameters for a desired motor, impact of limiting antenna acceleration, gear non-linearities, and the impact of the antenna hitting the gimbal stops. This paper has explored the theoretical groundwork for implementation of a sliding mode controller in a missile gimbal system.

REFERENCES

[1] V. I. Utkin, "*Sliding Modes in Control Optimization*", Berlin: Springer-Verlag, 1992.

[2] R. A. Decarlo, S. H. Zak, G. P. Matthews, "*Variable Structure Control of Nonlinear Multivariable Systems: A Tutorial*", *Proc. IEEE*, Vol 76, No. 3, pp 212-232, 1988.

[3] G. Stimson, "*Airborne Radar*", El Segundo, CA: Hughes Aircraft Company, 1983.

[4] "*Reference Data for Radio Engineers, fourth edition*", International Telephone and Telegraph Corporation, 1956.

[5] Y. B. Shtessel, "*Decentralized Sliding Mode Control in Three-Axis Inertial Platforms*", *Journal of Guidance Control, and Dynamics*, vol 18 no. 4, 1995, pp 773-781.

[6] D. T. Greenwood, "*Principles of Dynamics*", Englewood Ciffs: Prentice-Hall, 1965.

[7] M. W. Spong, M. Vidyasager, "*Robot Dynamics and Control*", New York: John Wiley & Sons, 1989.

[8] Y. B. Shtessel, "*Nonlinear Output Tracking Via Nonlinear Dynamic Sliding Manifolds*," *Proceedings of the 1994 International Symposium on Intelligent Control* (Columbus, OH), IEEE Control Systems Society, 1994, pp 297-302.

[9] J. J. Slotine, W. Li, "*Applied Non-Linear Control*", Englewood Cliffs: Prentice-Hall, 1991.

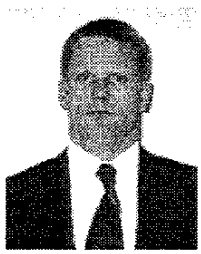

Brian J. Smith *is an electronics engineer with the Systems Simulation & Development Directorate, Missile Research, Development and Engineering Center, US AMCOM. He has worked in modeling and simulation of Air Defense Systems, Anti-Radiation Missiles, data comp-ression, and battlefield commun-ications systems. He has conducted extensive research in localized computerized tomography for medical imaging and defense related areas. He has a Ph.D. in Electrical and Computer Engineering from The University of Alabama in Huntsville.*

William J. Schrenk *is an electronics engineer with the Systems Simulation & Development Directorate, Missile Research, Development and Engineering Center, US AMCOM. He has over 20 years experience in Anti Radiation Missile counter- measures experience covering all US Air Defense Systems. He has a BSE, Electrical and Computer Engineering from The University of Alabama in Huntsville and is a registered Professional Engineer.*

Willam B. Gass *is an electronics engineer with the Systems Simulation & Development Directorate, Missile Research, Development and Engineering Center, US AMCOM. He has worked on the development of constructive and engineering level simulations of Army Air Defense Systems for real-time and non-real time applications. He has a B.S. in Electrical Engineering from Tennessee Tech University.*

Yuri B. Shtessel *received his M.S. and Ph.D. degrees in Electrical Engineering from the Chelyabinsk State Technical University, Chelyabinsk, Russia, in 1971 and 1978, respectively. In 1979-1991 he was with the Department of Applied Mathematics at the Chelyabinsk State Technical University. In 1991-1993 he was with the Department of Electrical and Computer Engineering at the University of South Carolina, Columbia, SC. Since 1993 he has been with the Department of Electrical and Computer Engineering at the University of Alabama in Huntsville. His research interests include sliding mode control with applications to flight and space control and autonomous systems of electric power supply. He published over 100 technical papers.*